*J. Fluid Mech.* (2007), *vol.* 588, *pp.* 463–473.  
doi:10.1017/S0022112007006829 Printed in the United Kingdom

# Ageostrophic instabilities in a horizontally uniform baroclinic flow along a slope

GEORGI. G. SUTYRIN

Graduate School of Oceanography, University of Rhode Island, Narragansett, RI 02882, USA

(Received 25 December 2006 and in revised form 14 May 2007)

The normal modes of a horizontally uniform, vertically sheared flow over a sloping bottom are considered in two active layers underneath a deep motionless third layer. The variations of the layer thickness are assumed to be small to analyse the sixth-order eigenvalue problem for finite-Froude-number typical for oceanic currents. The dispersion curves for the Rossby waves and the Poincaré modes of inertia–gravity waves (IGW) are investigated to identify the different types of instabilities that occur if there is a pair of wave components which have almost the same Doppler-shifted frequency related to crossover of the branches when the Froude number increases. Simple criteria for ageostrophic instabilities due to a resonance between the IGW and the Rossby wave because of the thickness gradient in either the lower or middle layer, are derived. They exactly correspond to violation of sufficient Ripa's conditions for the flow stability. In both cases the growth rate and the interval of unstable wavenumbers are shown to be proportional to the square root of the corresponding gradient of the layer thickness. These types of ageostrophic instability can coexist (and with Kelvin–Helmholtz instability). However, their role in generating unbalanced motions and mixing processes in geophysical fluids appears limited due to small growth rates and narrow intervals of the unstable wavenumbers in comparison to Kelvin–Helmholtz instability.

## 1. Introduction

Stratified rotating flows support various types of instabilities which can be interpreted in terms of resonances between different wave modes (Hayashi & Young 1987). Three major types of resonances between inertia–gravity waves (IGW) and the Rossby wave modes are known for horizontally uniform, vertically sheared flows (Sakai 1989). First, the kinetic energy of the mean flow is the most important for Kelvin–Helmholtz (K-H) instability due to high-frequency resonances between IGW modes at order-one Froude number. It provides mixing at small scales and has been studied mainly in a non-rotating frame.

The available part of the potential energy is a source of baroclinic instability which can be interpreted as vertical coupling between Rossby waves related to gradients of the basic potential vorticity (Cushman-Roisin 1994). Because the Rossby waves typically have low frequencies, most of these studies were done in a framework of quasi-geostrophic dynamics at small Froude and Rossby numbers when IGW are excluded *a priori*. The mechanism of this instability is most simply illustrated by the geostrophic two-layer Phillips model where the variations of layer thickness are small (Phillips 1954).

An ageostrophic version of Phillips' model (two-layer channel model on an *f*-plane with large variations of the layer thickness) was used to reveal a third type of instability (Orlanski 1968), which has been recognized as an instability caused by resonance between IGW and Rossby modes (Sakai 1989). It was found at finite Froude number and called the Rossby–Kelvin (R-K) instability to indicate the different types of waves that resonate in the lowest mode. The instability occurs if there is a pair of IGW and Rossby wave components which propagate in the opposite direction to the basic flow and which have almost the same Doppler-shifted frequency. In the R-K instability the Rossby waves are almost in geostrophic balance while the ageostrophic IGW are the same as in a one-layer system. Doppler shifting matches frequencies which would otherwise be very different.

R-K-type instability is also found in a continuously stratified model (ageostrophic version of the Eady model). Stone (1966, 1970) found some unstable modes with phase speed different from that of the average basic flow (note that the conventional baroclinic instability has the same phase speed as the average basic flow). This instability is identified by Nakamura (1988) as due to the inertial critical layer. He showed that this unstable mode is caused by an interaction between a vorticity mode trapped at the boundary and an IGW mode which has intrinsic frequency of order the Coriolis parameter and is trapped in the inertial critical layer (see also Plougonven, Muraki & Snyder 2005). Recently Molemaker, McWilliams & Yavneh (2005) have investigated R-K-type instability in a continuously stratified model with an emphasis on how it relates to the breakdown of balance in the neighbourhood of loss of balanced integrability and on how its properties compare with examples of ageostrophic anticyclonic instability of rotating, stratified, horizontally sheared currents.

Here we consider a multi-layer ageostrophic version of Phillips' model for spatially uniform flow over sloping topography in a configuration with small variations of layer thickness which allows to consider analytically all the types of instability mentioned (Kelvin–Helmholtz, Rossby–Kelvin, baroclinic) in approximated systems of ordinary differential equations (ODEs) with constant coefficients. The dispersion curves and wave resonances can be analysed explicitly, which helps to distinguish ageostrophic R-K instabilities related to a gradient of potential vorticity in each layer. In § 2, basic equations for a two-and-half-layer system are described, Ripa's stability conditions are considered and the eigenproblem is formulated for linearized equations. In § 3, different IGW modes are analysed in connection with K-H instability. In § 4, the Rossby waves and R-K instabilities are described in detail. In § 5, examples of transformation of dispersion curves with increasing Froude number are provided. In § 6, the results are summarized and discussed.

## 2. Mathematical formulation

### 2.1. *The two-active-layer model*

Let us consider a three-layer, inviscid, rotating fluid in a channel of width $2L$ with a linearly sloping bottom. The layer densities are $\rho_j$, the depths are $H_j$, the pressure field is $P_j$, and the velocity vector is $\boldsymbol{V}_j = (U_j, V_j)$, where $j = 1$, $j = 2$ and $j = 3$ represent variables in the lower, middle and upper layer, respectively (see figure 1). The right-hand coordinate system corresponds to the depth topography $H(X)$, with the $X$-axis directed onshore, and the $Y$-axis parallel to the isobath; $t$ is time.

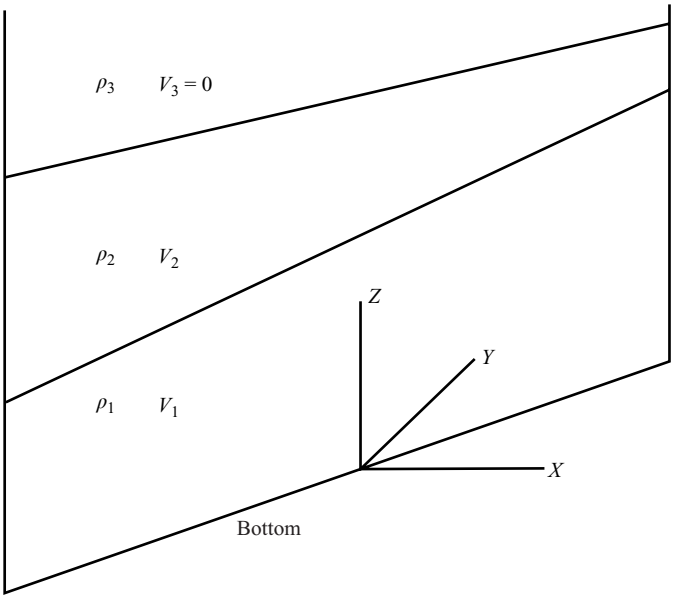


FIGURE 1. The three-layer baroclinic flow configuration along a sloping bottom in a channel.

First, we non-dimensionalize the variables as follows:

$$(\hat{X}, \hat{Y}) = (X, Y) f_0 / V_0, \qquad \hat{t} = t f_0, \tag{1}$$

$$(\hat{U}_j, \hat{V}_j) = (U_j, V_j)/V_0, \qquad \hat{H}_j = H_j/H_0, \qquad \hat{P}_j = P_j/\rho_1 V_0^2, \tag{2}$$

where $V_0 = \sqrt{g' H_0}$ is the characteristic velocity, $H_0$ is the characteristic layer depth, $g' = g(\rho_1 - \rho_2)/\rho_1$ is the reduced gravity, and $f_0$ is the Coriolis parameter.

In the Boussinesq, hydrostatic, and $f$-plane approximations the non-dimensional momentum and continuity equations are

$$\partial_t \boldsymbol{V}_j + (\boldsymbol{V}_j \cdot \nabla)\boldsymbol{V}_j + \boldsymbol{k} \times V_j = -\nabla P_j, \tag{3}$$

$$\partial_t H_j + \nabla \cdot (H_j \boldsymbol{V}_j) = 0, \tag{4}$$

where $\nabla$ is the horizontal gradient operator, $\boldsymbol{k}$ is the vertical unit vector, and the hats for the non-dimensional variables are dropped. Here we assume $\rho_1 - \rho_3 \ll \rho_1$. The pressure and layer thickness gradients are related by the hydrostatic equations:

$$\nabla(H_1 + H(X)) = \nabla(P_1 - P_2), \qquad \nabla(H_1 + H(X) + H_2) = \gamma \nabla(P_2 - P_3), \tag{5}$$

where $\gamma = (\rho_1 - \rho_2)/(\rho_2 - \rho_3)$. The limit $\gamma = 0$ corresponds to a widely used rigid-lid two-layer model. Further we assume the upper layer to be infinitely deep and motionless ($P_3 = 0$) to analyse the coupling of the middle and lower active layers for finite $\gamma$.

### 2.2. *The basic state and stability conditions*

We consider the basic state with horizontally uniform flows in each layer:

$$U_j = 0, \qquad V_j = \frac{\mathrm{d}P_j}{\mathrm{d}X}, \qquad H_j = \overline{H}_j + S_j X, \qquad S_1 = V - S, \qquad S_2 = \gamma V_2 - V, \tag{6}$$

where $S$ is the topographic slope and $V = V_1 - V_2$ characterizes the Froude number. Further we assume $V > 0$ and choose the coordinates moving with the middle layer

velocity $V_2$. According to general stability conditions for a two-and-half-layer model given in table 2 in Ripa (1991), this parallel flow is stable if there exists any value of a constant $a$ such that

$$(V-a)S_1<0, \qquad aS_2>0, \qquad F_1(1-\gamma F_2)+(1+\gamma)F_2<1, \qquad \gamma F_2<1, \quad (7)$$

where $F_1=(V-a)^2/H_1$, $F_2=a^2/H_2$. When $S_1=S_2=0$, the first two conditions are irrelevant, while the last two conditions in (7) can be violated for $V>V_{KH}$ corresponding to the K-H instability (see § 3).

In our configuration two types of the R-K instability can be analysed independently: one is related to the Rossby mode due to the lower-layer thickness gradient, another is related to the Rossby mode due to the middle-layer thickness gradient. When $S_1>0$ and $S_2\geqslant 0$, the first two conditions give $a>V$, then the last two conditions can be violated for $(1+\gamma)V^2>H_2$, corresponding to the R-K instability described in § 4.1. When $S_1\leqslant 0$ and $S_2<0$, the first two conditions give $a<0$, then the last two conditions can be violated when $V^2>H_1$, corresponding to R-K instability described in § 4.2.

When $S_1>0$ and $S_2<0$, the first two conditions give $a>V$ and $a<0$ that cannot be satisfied, corresponding to conventional baroclinic instability considered in § 4.3. When $S_1<0$ and $S_2>0$ the first two conditions are satisfied for $0<a<V$, then the last two conditions could be violated only for K-H instability. It is an example of when the Rayleigh criterion of opposite sign for gradients of potential vorticity in two layers necessary for instability is not sufficient.

### 2.3. *Linearization*

The linear stability of this flow is addressed by adding infinitesimal disturbances of the form $(\mathrm{i}u_j(X), v_j(X), p_j(X))\exp(\mathrm{i}kY-\mathrm{i}\omega t)$ and linearizing. Here $k$ is the disturbance wavenumber and $\omega$ is the disturbance frequency (a positive imaginary part implying instability). The linearized equations (3)–(5) are

$$\sigma_1 u_1 - v_1 + p_1' = 0, \qquad u_1 - \sigma_1 v_1 + kp_1 = 0, \quad (8)$$

$$\sigma_1(p_2-p_1)+(H_1u_1)'+kH_1v_1=0, \quad (9)$$

$$\sigma_2 u_2 - v_2 + p_2' = 0, \qquad u_2 - \sigma_2 v_2 + kp_2 = 0, \quad (10)$$

$$\sigma_2(p_1-p_2-\gamma p_2)+(H_2u_2)'+kH_2v_2=0, \quad (11)$$

where intrinsic frequencies $\sigma_1=\omega-kV$, $\sigma_2=\omega$, and $'$ denotes $\mathrm{d}/\mathrm{d}X$. The system (8)–(11) is a sixth-order eigenvalue problem to be solved with the boundary conditions $u_j=0$ at $X=\pm L$ to obtain a set of normal modes which are orthogonal to each other in an appropriate norm. From (8) and (10) we can express $(u_j, v_j)$ via $p_j$ as

$$f_j u_j = \sigma_j p_j' - kp_j, \qquad f_j v_j = p_j' - \sigma_j k p_j, \qquad f_j = 1-\sigma_j^2. \quad (12)$$

Then from (9) and (11) we obtain two coupled second-order ODEs for $p_j(X)$:

$$f_1(p_1-p_2)+(\overline{H}_1+S_1X)(k^2p_1-p_1'')-S_1p_1' = -\frac{k}{\sigma_1}S_1p_1, \quad (13)$$

$$f_2(\gamma p_2+p_2-p_1)+(\overline{H}_2+S_2X)(k^2p_2-p_2'')-S_2p_2' = -\frac{k}{\sigma_2}S_2p_2, \quad (14)$$

with the boundary conditions obtained from (12):

$$\sigma_j p_j' = kp_j \qquad \text{at} \qquad X=\pm L. \quad (15)$$

The system (13)–(15) describes four sets of the IGW and two sets of the topographic Rossby wave, depending on the Froude number, $V$, the depth ratio, $\overline{H}_1/\overline{H}_2$, the density ratio, $\gamma$, the channel width, $L$, and two depth gradients, $S_j$. Generally, eigenvalues and eigenfunctions can be found numerically by discretizing the $X$-interval. In order to analyse different modes and their resonances explicitly, we further assume that the changes in thickness of both layers are small $|S_j| \ll 1$.

## 3. Inertia–gravity modes

The Rossby modes are absent if $S_1 = S_2 = 0$, i.e. $V = S = \gamma V_2$; then only K-H instability is possible due to vertical shear. In this case the coefficients in coupled ODEs (13)–(14) become constant:

$$f_1 p_1 + \overline{H}_1(k^2 p_1 - p_1'') = f_1 p_2, \qquad f_2 p_1 = (\gamma + 1) f_2 p_2 + \overline{H}_2(k^2 p_2 - p_2''), \tag{16}$$

and we seek the solution to (16) in the form of periodic Poincaré modes satisfying (15)

$$p_j = Z_j \sin(\alpha X + \phi_j) + \text{c.c.}, \qquad \alpha = \frac{\pi m}{2L}, \qquad \tan\{\phi_j + [1-(-1)^m]\pi/4\} = \frac{\sigma_j \alpha}{k}, \tag{17}$$

where $Z_j$ are amplitudes, $m$ is the modal number, and c.c. means complex conjugate. (Here we exclude from consideration the boundary-trapped Kelvin modes of IGW analysed by Sakai (1989)). Then from (16) we obtain the matrix equation for $(Z_1, Z_2)$ and its determinant has the form of the forth-order algebraic equation corresponding to the boundary of Ripa's third condition (7) for $F_j = (\sigma_j^2 - 1)/Q_j$:

$$1 + \gamma \frac{(\sigma_1^2 - 1)(\sigma_2^2 - 1)}{Q_1 Q_2} = \frac{\sigma_1^2 - 1}{Q_1} + (1 + \gamma)\frac{\sigma_2^2 - 1}{Q_2}, \qquad Q_j = \overline{H}_j(k^2 + \alpha^2). \tag{18}$$

Without vertical shear and over a flat bottom, $V = S = 0$, we have $\sigma_1 = \sigma_2 = \omega$; then (18) describes four branches of a neutral IGW for two internal modes, $\omega_n^2 = 1 + (k^2 + \alpha^2)C_n^2$:

$$C_1^2 = \frac{1}{2\gamma}[\overline{H}_2 + (1 + \gamma)\overline{H}_1 + \sqrt{D}], \qquad C_2^2 = \frac{2\overline{H}_1\overline{H}_2}{\overline{H}_2 + (1 + \gamma)\overline{H}_1 + \sqrt{D}}, \tag{19}$$

where $D = (\overline{H}_2 + (1 + \gamma)\overline{H}_1)^2 - 4\gamma\overline{H}_1\overline{H}_2$. The internal-mode speed ratio depends on $\mu$:

$$\frac{C_1}{C_2} = \sqrt{\frac{2}{\mu}(1 + \sqrt{1 - \mu}) - 1}, \qquad \mu = \frac{4\gamma\delta(1 - \delta)}{(1 + \gamma\delta)^2}, \tag{20}$$

where $\delta = \overline{H}_1/(\overline{H}_1 + \overline{H}_2)$ is the depth ratio. We see that $\mu \ll 1$ when either $\gamma \ll 1$ (the limit of a rigid-lid upper interface), or $\gamma \gg 1$ (the limit of an inactive middle layer), or $\delta \to 1$ (small middle-layer thickness), or $\delta \ll 1$ (small lowe-layer thickness). In all these cases the first internal–gravity mode propagates much faster than the second mode ($C_1 \gg C_2$).

When analysing the flow instability for $V > 0$, we use an asymptotic expansion in $\gamma$ assuming $\omega = \omega_0 + \gamma\omega_1 + \cdots$. At the leading order, setting $\gamma = 0$ in (18), we obtain

$$\omega_0^2(Q_1 + Q_2) - 2\omega_0 k V Q_2 + k^2 V^2 Q_2 - Q_1 - Q_2 - Q_1 Q_2 = 0, \tag{21}$$

which gives the condition of K-H instability in the rigid-lid two-layer system for the gravest mode with $\alpha \ll 1$ when $Q_j \approx k^2 \overline{H}_j$:

$$V^2 > \overline{H}_1 + \overline{H}_2 + \frac{(\overline{H}_1 + \overline{H}_2)^2}{\overline{H}_1 \overline{H}_2 k^2}, \qquad \omega_{0i} = \sqrt{\frac{k^2 V^2 \overline{H}_1 \overline{H}_2}{(\overline{H}_1 + \overline{H}_2)^2} - \frac{k^2 \overline{H}_1 \overline{H}_2}{\overline{H}_1 + \overline{H}_2} - 1}, \tag{22}$$

where the growth rate $\omega_{0i}$ increases with the wavenumber $k$. One can see that in the short-wave limit this instability condition $V^2 > \overline{H}_1 + \overline{H}_2$ corresponds to violation of Ripa's third condition (7): $F_1 + F_2 < 1$ for $\gamma = 0$.

Taking into account the next order in $\gamma$, we find that this high-frequency instability is possible only for the Froude number $V > V_{KH}$ where

$$V_{KH} = \sqrt{\overline{H}_1 + \overline{H}_2 - \frac{\gamma \overline{H}_2^2}{\overline{H}_1 + \overline{H}_2} + O(\gamma^2)}. \tag{23}$$

## 4. The Rossby waves and ageostrophic R-K instability

### 4.1. *The Rossby mode due to the lower-layer thickness gradient*

When only $S_2 = 0$, (13)–(15) becomes the fifth-order eigenvalue problem. Owing to the smallness of $S_1$ the topographic Rossby wave branch can be described in the quasigeostrophic approximation, assuming $f_1 = f_2 \approx 1$ to filter out the IGW, and neglecting small terms proportional to $S_1$ in the left-hand side of (13) to obtain the equation with constant coefficients

$$p_1 - p_2 + H_1(k^2 p_1 - p_1'') = -\frac{S_1 p_1}{c_1}, \tag{24}$$

where $c_1 = \omega/k - V$. Then the solution in the form (17) gives

$$c_1 = -S_1 \frac{1 + \gamma + Q_2}{\gamma + Q_2 + Q_1(1 + \gamma + Q_2)}. \tag{25}$$

Thus, the Doppler-shifted intrinsic phase speed of the Rossby wave, $c_1$, is small and to consider its resonance with the IGW mode we take into account only the leading-order correction to $f_2 = 1 - k^2(V + c_1)^2 \approx 1 - k^2 V^2 - 2k^2 V c_1$ in (14):

$$(1 - k^2 V^2 - 2k^2 V c_1)(p_1 - \gamma p_2 - p_2) = H_2(k^2 p_2 - p_2''). \tag{26}$$

Then seeking the solution in the form (17) to (24) and (26) gives a quadratic equation for $c_1$ which describes the branches of the Doppler-shifted Rossby wave and IGW in the vicinity of $\omega \approx kV$:

$$A_1 c_1^2 - B_1 c_1 = S_1[(1 + \gamma)(1 - k^2 V^2) + Q_2], \qquad c_1 = \frac{B_1 \pm \sqrt{D_1}}{2A_1}, \tag{27}$$

$$A_1 = 2k^2 V(\gamma + Q_1 + \gamma Q_1), \qquad B_1 = Q_2 + Q_1 Q_2 + (Q_1 + \gamma + \gamma Q_1)(1 - k^2 V^2), \tag{28}$$

$$D_1 = B_1^2 + 8k^2 V S_1(Q_1 + \gamma + \gamma Q_1)[Q_2 + (1 + \gamma)(1 - k^2 V^2)]. \tag{29}$$

The two branches are able to cross in the vicinity of the resonant wavenumber $k_1$ given by the condition $B_1 = 0$, which can be written as a quadratic equation for $K_1^2 = k_1^2 + \alpha^2$:

$$\overline{H}_2 K_1^2 + \overline{H}_1 \overline{H}_2 K_1^4 + \left[\gamma + (1 + \gamma)\overline{H}_1 K_1^2\right]\left[1 - \left(K_1^2 - \alpha^2\right)V^2\right] = 0. \tag{30}$$

In agreement with violation of Ripa's third stability condition (7) for $a = V$, such a resonant wavenumber exists when $A_K \equiv (1+\gamma)V^2 - \overline{H}_2 > 0$:

$$K_1^2 = \frac{B_K + \sqrt{D_K}}{2\overline{H}_1 A_K}, \tag{31}$$

$$B_K = (1+\alpha^2V^2)(1+\gamma)\overline{H}_1 + \overline{H}_2 - \gamma V^2, \qquad D_K = B_K^2 + \gamma\overline{H}_1 A_K(1+\alpha^2V^2). \tag{32}$$

The resonance appears at infinitely large wavenumber when $A_K$ becomes positive and $K_1$ decreases as $V$ increases further.

The imaginary part of $c_1$ could be non-zero within the unstable wavenumber interval $k_1 - \kappa_m < k < k_1 + \kappa_p$ defined by $D_1(k_1 - k_m) = D_1(k_1 + k_p) = 0$ if

$$D_1(k_1) = -8k_1^2K_1^2\overline{H}_2 V S_1 < 0, \tag{33}$$

which is possible only if $VS_1 > 0$, i.e. when the Rossby wave propagates upstream in the lower layer in agreement with violation of Ripa's stability conditions (7) and the analysis by Sakai (1989). The corresponding R-K instability has the maximum growth rate proportional to $\sqrt{S_1/V}$:

$$\omega_i = k_1 c_{1i} = \sqrt{\frac{S_1\overline{H}_2}{2V}}\frac{K_1}{\gamma + (1+\gamma)\overline{H}_1K_1^2}, \tag{34}$$

which confirms the validity of neglecting the terms proportional to $S_1 \simeq c_1^2$ in the left-hand side of (13). One can see from (27)–(29) that the interval of unstable wavenumbers $\kappa_p + \kappa_m$ is proportional to $\sqrt{S_1 V}$ and $\kappa_p + \kappa_m$ decreases when $V$ increases.

### 4.2. *The Rossby wave due to the middle-layer thickness gradient*

When $S_1 = 0$ and $S_2 < 0$, the phase speed of the topographic Rossby wave is also small due to the smallness of $|S_2|$. To consider its resonance with the IGW mode we approximate $f_1 = 1 - k^2(c-V)^2 \approx 1 - k^2V^2 + 2k^2Vc$, $f_2 = 1 - k^2c^2 \approx 1$, and neglect small terms proportional to $S_2$ in the left-hand side of (14), taking into account only the leading order in $c$. Then the solution to (13)–(14) in the form (17) gives a quadratic equation for $c$ similar to (27)–(29) which describes here branches of the Rossby wave and Doppler-shifted IGW in the vicinity of $\omega = 0$. These branches are able to cross in the vicinity of the resonant wavenumber $k_2$, which can be written as a quadratic equation for $K_2^2 = k_2^2 + \alpha^2$:

$$(1+\gamma)\overline{H}_1K_2^2 + \overline{H}_1\overline{H}_2K_2^4 + \left(\gamma + \overline{H}_2K_2^2\right)\left[1 - \left(K_2^2 - \alpha^2\right)V^2\right] = 0. \tag{35}$$

In agreement with violation of Ripa's third condition (7) for $a = 0$, such a resonant wavenumber exists when $V^2 > \overline{H}_1$. The imaginary part of $c$ at $k = k_2$ is non-zero if $VS_2 < 0$, i.e. when the Rossby wave in the middle layer propagates downstream relative the flow in the lower layer. The corresponding R-K instability has maximum growth rate proportional to $\sqrt{-S_2/V}$:

$$\sigma_i = k_2 c_i = \sqrt{\frac{-S_2\overline{H}_1}{2V}}\frac{K_2}{\gamma + \overline{H}_2K_2^2}. \tag{36}$$

In this case, the interval of unstable wavenumbers is proportional to $\sqrt{-S_2V}$.

Both types of R-K instability have the same resonant wavenumbers, $k_1 = k_2$, and growth rates when $\overline{H}_1 = \overline{H}_2$, $S_1 = -S_2$, and $\gamma = 0$, corresponding to the configuration considered by Sakai (1989). Note that the first Poincaré mode of R-K instability is seen in his figure 6 for the Froude number $F > 0.7$, defined as $F = V/2C_2$ with

$C_2 = \sqrt{\overline{H}_1/2}$, which agrees well with the condition $V > \sqrt{\overline{H}_1}$ obtained here. Such instabilities are similar to the topographic Rossby wave–IGW instability in spatially localized gravity currents along a slope considered by Meacham & Stephens (2001) as well as to the subsynoptic-scale baroclinic instability identified by Yamazaki & Peltier (2001).

### 4.3. *Geostrophic baroclinic instability*

Finally, when the thickness varies in both layers, two types of ageostrophic R-K instability can coexist (see § 5). In addition, coupling between two Rossby wave branches provides baroclinic instability if $S_1 V > 0$ and $S_2 V < 0$, which have been intensively studied in the past in the limit of low frequency $|\sigma| \ll 1$ and small Rossby number $kV \ll 1$. In this case filtering out the IGW by assuming $f_1 \simeq f_2 \simeq 1$ and neglecting small terms proportional to either $S_1$ or $S_2$ in the left-hand side of (13)–(14) gives

$$p_1 + H_1(k^2 p_1 - p_1'') + \frac{S_1 p_1}{c_1} = p_2, \qquad (1+\gamma)p_2 + H_1(k^2 p_2 - p_2'') + \frac{S_2 p_2}{c_2} = p_1. \quad (37)$$

Seeking the solution to (37) in the form (17) gives a quadratic dispersion equation:

$$c(c-V)[(\gamma+Q_2)(1+Q_1)+Q_1]+(c-V)S_2(1+Q_1)+cS_1(1+\gamma+Q_2)+S_1S_2 = 0. \quad (38)$$

Such baroclinic instability arises due to a resonance between the Rossby waves related to the thickness gradient in the middle and lower layers, analysed in the three-layer quasi-geostrophic model in detail by Pichevin (1998).

In particular, the stability characteristics of the pure baroclinic Swaters' mode for a wedge flow configuration along the slope can be obtained from (38) in the limit of $\gamma \to 0$, $Q_1 \to 0 (\overline{H}_1 \ll \overline{H}_2)$ and $S_2 = -V$:

$$Q_2 c^2 - (V - S_1)(1 + Q_2)c + V^2 - V S_1 = 0, \quad (39)$$

$$c = 2V \frac{1 \pm \sqrt{1-\chi}}{\chi(1+Q_2)}, \qquad \chi = \frac{4VQ_2}{(V-S_1)(1+Q_2)^2}. \quad (40)$$

Here the instability condition $\chi > 1$ coincides with (3.12) of Mooney & Swaters (1996) when $S_1 \ll V$, while the growth rate and the interval of unstable wavenumbers are also proportional to $\sqrt{S_1}$ as for the R-K instability considered above.

## 5. Transformation of dispersion curves

In order to illustrate how the dispersion curves evolve when vertical shear increases, while the changes in thickness of both layers remain small, $|S_j| \ll 1$, we neglect only small terms proportional to either $S_1$ or $S_2$ in the left-hand side of (13)–(14) and seek the solution in the form (17). Then we obtain the matrix equation $\boldsymbol{M} \cdot \boldsymbol{Z} = 0$ where

$$\left.\begin{aligned} M_{11} &= f_1 + Q_1 + \frac{kS_1}{\sigma_1}, \qquad M_{12} = -f_1, \\ M_{21} &= -f_2, \qquad M_{22} = (1+\gamma)f_2 + Q_2 + \frac{kS_2}{\sigma_2}, \end{aligned}\right\} \quad (41)$$

so that the determinant of (41) can be written as

$$\frac{\sigma_1\sigma_2}{k^2}[(\gamma f_2+Q_2)(f_1+Q_1)+f_2Q_1]+\frac{\sigma_1 S_2}{k}(f_1+Q_1)+\frac{\sigma_2 S_1}{k}[(1+\gamma)f_2+Q_2] = -S_1S_2. \quad (42)$$

Examples of dispersion curves calculated for increasing Froude number $0 \leqslant V \leqslant 1$ from (42) for $\overline{H}_1 = \overline{H}_2 = 0.5$, $\gamma = 1$, $S_1 = -S_2 = 0.2$, $\alpha = 1$ are shown in figure 2. The

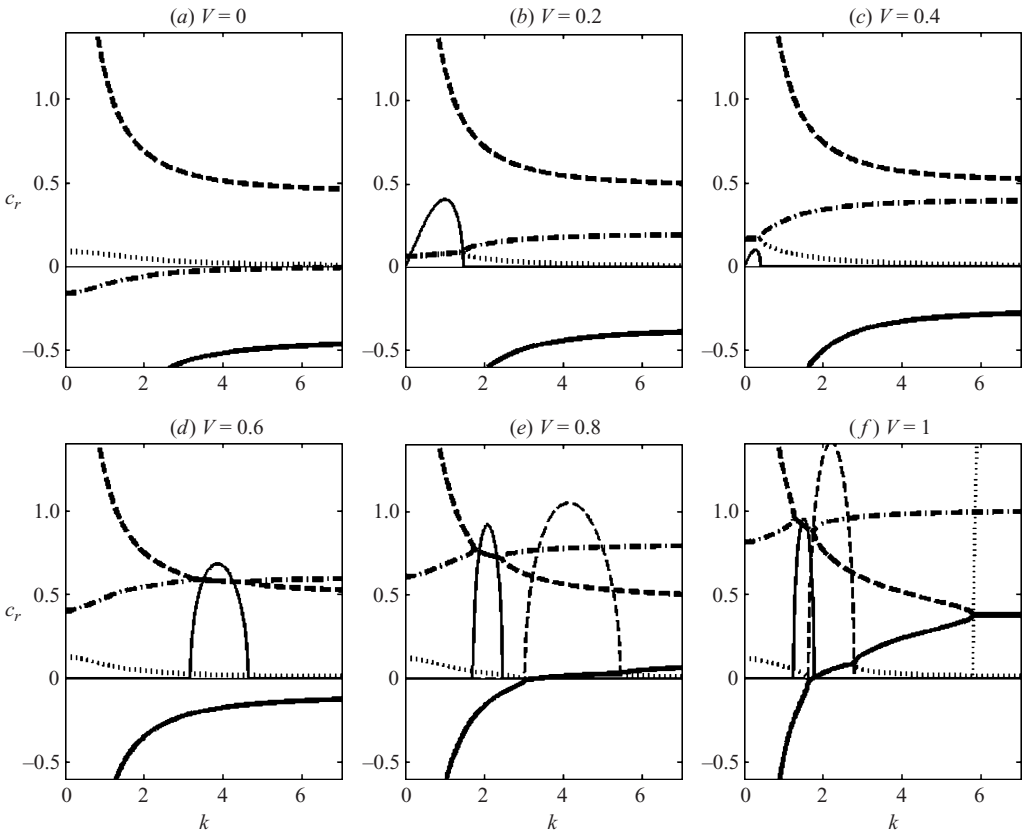


FIGURE 2. The real part of the phase velocity for the second IGW modes (downstream propagating, dashed and upstream propagating, solid curves) and the Rossby wave modes (downstream propagating, dotted and upstream propagating, dash-dotted curves) depending on the wavenumber $k$ according to (17) for $\overline{H}_1 = \overline{H}_2 = 0.5; \gamma = 1; S_1 = -S_2 = 0.2; \alpha = 1$ and six values of $V$. The growth rates (multiplied by 10) corresponding to crossover of the branches are shown for the baroclinic instability (thin solid line in (*b*) and (*c*)), R-K instability (thin solid and dashed lines in (*d*), (*e*), (*f*)), and K-H instability (thin dotted line in (*f*)).

phase speed $c_r$ is shown for the second IGW modes (downstream propagating, dashed line, and upstream propagating, solid line) as well as for the upstream-propagating Rossby wave, dash-dotted line, related to $S_1 > 0$ in the lower layer, and the downstream-propagating Rossby wave, dotted line, related to $S_2 < 0$ in the middle layer.

When $V = 0$ (figure 2*a*), the phase speed of topographic Rossby waves is much smaller than that of IGW modes. When $V = S_1$ (figure 2*b*), the conventional baroclinic instability has the maximum growth rate given by (38) at $k \approx 1$ due to resonance between Doppler-shifted Rossby waves within the interval of unstable wavenumbers $0 \leqslant k \leqslant 1.8$. When $V = 0.4$ (figure 2*c*), the upstream-propagating Rossby wave has larger Doppler shift, so that the baroclinic instability growth rate and the interval of unstable wavenumbers are much smaller.

When $V = 0.6 > \sqrt{\overline{H}_2/(1+\gamma)} = 0.5$ (figure 2*d*), ageostrophic R-K instability becomes possible due to a resonance between the Rossby mode related to the lower-layer thickness gradient and the downstream-propagating IGW with the maximum

growth rate described by (34), while the Doppler shift becomes too large for a resonance between the Rossby waves. When $V = 0.8 > \sqrt{\overline{H}_1} = 0.7$ (figure 2*e*), another R-K instability becomes possible due to a resonance between the Rossby mode related to the middle-layer thickness gradient and the Doppler-shifted upstream-propagating IGW with the maximum growth rate given by (36); it coexists here with the first R-K instability in a more narrow interval of unstable wavenumbers.

Finally, when $V = 1$ (figure 2*f*), K-H instability becomes possible for $k > 6$ in agreement with (23); it coexists here with both types of the R-K instabilities which unstable wavenumber intervals become to overlapping.

## 6. Discussion and conclusions

A multi-layer ageostrophic version of Phillips' model over sloping topography with small variations of the layer thickness allows consideration of analytically different types of instability (Kelvin–Helmholtz, Rossby–Kelvin, baroclinic) in horizontally uniform flows. The dispersion curves for the Rossby waves and IGW are investigated for a two-and-half-layer configuration to identify different instabilities related to crossover of the branches when the Froude number increases. Simple criteria for R-K-type ageostrophic instabilities are found: either $(1+\gamma)V^2 > \overline{H}_2$ due to a resonance between the IGW modes and the Rossby wave when $VS_1 > 0$, or $V^2 > \overline{H}_1$ due to a resonance with the Rossby wave when $VS_2 < 0$. They exactly correspond to violation of sufficient conditions for the flow stability (Ripa 1991). In both cases the growth rate (and the interval of unstable wavenumbers in the vicinity of the resonant wavenumber) are shown to be proportional to the square root of the corresponding gradient of the layer thickness.

As mentioned by Sakai (1989), ageostrophic instabilities in horizontally sheared flows can be interpreted in the present context as resonance between different Rossby, IGW, and trapped Kelvin modes (e.g. Griffiths, Killworth & Stern 1982; Ford 1993; McWilliams, Molemaker & Yavneh 2004). In such cases, the waves interact horizontally in contrast to the vertical interaction in the R-K instability discussed above. However, even for order-one Rossby number, the growth rates of ageostrophic instabilities in horizontally sheared flows are typically quite small (less than 5 % of $f$).

The dispersion curves demonstrate that R-K types of ageostrophic instability related to the thickness gradient in different layers can coexist together (and with Kelvin–Helmholtz instability) and their growth rates may exceed the growth rates of conventional baroclinic instability (figure 2). Nevertheless, the growth rates of R-K instabilities are within 10 % of $f$, and are much smaller than the growth rates of K-H instability and their intervals of unstable wavenumbers are much narrower. Such inefficiency of resonances between the Rossby and IGW modes in generating substantial unbalanced motions in varying baroclinic flows is consistent with the small-Rossby-number asymptotic analysis of Zeitlin, Reznik & Ben Jelloul (2003), who demonstrated a decoupling of balanced and imbalanced motions for long times, and with the astonishing persistent of balance demonstrated by McIntyre & Norton (2000) in the shallow-water model on a hemisphere and by Dritschel & Viudez (2007) in baroclinically unstable stratified flows.

Further investigations are needed to clarify finite-amplitude forms of ageostrophic instabilities and their relation to the breakdowns of balance in the agradient velocity model for finite Froude number (Sutyrin 2004) and in anticyclonically sheared flows for finite Rossby mumber (Molemaker *et al.* 2005).

The author is sincerely grateful for useful comments by Gordon Swaters and Gregory Reznik. This study was supported by the NSF Division of Ocean Sciences and by ONR, Ocean Science Division.

## REFERENCES

Cushman-Roisin, B. 1994 *Introduction to Geophysical Fluid Dynamics*. Prentice Hall.

Dritschel, D. G. & Viudez, A. 2007 The persistence of balance in geophysical flows. *J. Fluid Mech.* **570**, 365–383.

Ford, R. 1993 Gravity wave generation by vortical flows in a rotating frame. PhD Thesis, University of Cambridge.

Griffiths, R. W., Killworth, P. D. & Stern, M. E. 1982 Ageostrophic instability of ocean currents. *J. Fluid Mech.* **117**, 343–377

Hayashi, Y. Y. & Young, W. R. 1987 Stable and unstable shear modes of rotating parallel flows in shallow water. *J. Fluid Mech.* **184**, 477–504.

McIntyre, M. E. & Norton, W. A. 2000 Potential vorticity inversion on a hemisphere. *J. Atmos. Sci.* **57**, 1214–1235, and Corrigendum **58**, 949.

McWilliams, J. C., Molemaker, M. J. & Yavneh, I. 2004 Ageostrophic, anticyclonic instability of a geostrophic, barotropic boundary current. *Phys. Fluids* **16**, 3720–3725.

Meacham, S. P. & Stephens, J. C. 2001 Instabilities of gravity currents along a slope. *J. Phys. Oceanogr.* **31**, 30–53.

Molemaker, M. J., McWilliams, J. C. & Yavneh, I. 2005 Baroclinic instability and loss of balance. *J. Phys. Oceanogr.* **35**, 1505–1517.

Mooney, C. J. & Swaters, G. E. 1996 Finite-amplitude baroclinic instability of a mesoscale gravity current in a channel. *Geophys. Astrophys. Fluid Dyn.* **82**, 173–205.

Nakamura, K. 1988 The scale selection of baroclinic instability – effect of stratification and nongeostrophy. *J. Atmos. Sci.* **45**, 3253–3267.

Orlanski, I. 1968 Instability of frontal waves. *J. Atmos. Sci.* **25**, 178–200.

Pichevin, T. 1998 Baroclinic instability in a three layer flow: a wave approach. *Dyn. Atmos. Oceans* **28**, 179–204.

Phillips, N. A. 1954 Energy transformations and meridional circulations associated with simple baroclinic waves in a two-level, quasigeostrophic model. *Tellus* **6**, 273–286.

Plougonven, R., Muraki, D. J. & Snyder, C. 2005 A baroclinic instability that couples balanced motions and gravity waves. *J. Atmos. Sci.* **62**, 1545–1559.

Ripa, P. 1991 General stability conditions for a multi-layer model. *J. Fluid Mech.* **222**, 119–137.

Sakai, S. 1989 Rossby-Kelvin instability: a new type of ageostrophic instability caused by a resonance between Rossby waves and gravity waves. *J. Fluid Mech.* **202**, 149–176.

Stone, P. 1966 On non-geostrophic baroclinic stability. *J. Atmos. Sci.* **23**, 390–400.

Stone, P. 1970 On non-geostrophic baroclinic stability: Part 11. *J. Atmos. Sci.* **27**, 721–726.

Sutyrin, G. G. 2004 Agradient velocity, vortical motion and gravity waves in rotating shallow water model. *Q. J. R. Met. Soc.* **130**, 1977–1989.

Yamazaki, Y. H. & Peltier, W. R. 2001 The existence of subsynoptic-scale baroclinic instability and the nonlinear evolution of shallow disturbances. *J. Atmos. Sci.* **58**, 657–683.

Zeitlin, V., Reznik, G. M. & Ben Jelloul, M. 2003 Nonlinear theory of geostrophic adjustment. Part 2. Two-layer and continuously stratified primitive equations. *J. Fluid Mech.* **491**, 207–228.